EUROTHERM 82
Numerical Heat Transfer 2005
September 13-16, 2005 Gliwice-Kraków, Poland
Eds.: A. Nowak, R.A. Białecki

EXPERIMENTAL AND NUMERICAL INVESTIGATION OF NATURAL CONVECTION IN RECTANGULAR INCLINED ENCLOSURE

K. Dekajło*, T.A. Kowalewski

IPPT PAN, Department of Mechanics & Physics of Fluids, PL 00-049 Warszawa, Poland

Key words: natural convection, slope flow, rectangular enclosure cavity, numerical, experimental.

Abstract
The natural convection of water in inclined side-heated rectangular box was investigated both experimentally and numerically. The cavity had aspect ratio L/H = 3, the two opposite walls isothermal and kept at different temperatures, and four other walls adiabatic. The working fluid was water. The enclosure inclination φ varied from 0 to 90 deg. The Rayleigh number modified by cosφ varied in the range of $1\cdot10^6<Ra_y<7.5\cdot10^6$. Particle image velocimetry (PIV) and particle image thermometry (PIT) were used for quantitative analysis of the temporary velocity and temperature fields generated in the cavity. The numerical simulations of selected configurations were carried out and compared with the experimental data.

1. Introduction

The natural convection process has developed considerable importance because of its relevance to heat transfer in many engineering applications. These are: cooling of electronic components, heating and cooling of rooms, solar heaters, crystal growth, glass melting etc. The natural convection process inside rectangular enclosures has been studied extensively for the last four decades. S. Ostrach [1] has given a review of the history and developments of such heat transfer processes with the inception of convection as a research topic. The free convection plays also very important role in meteorology. Specifically, thermal circulation in a complex terrain is not yet fully understood and implemented in large scale atmospheric models. Theoretical models [2] and field observations [3] indicated presence of specific for the slope flow instabilities, like bellowing, "peeling off" and formation of stagnation fronts. These phenomena play an important role in a heat balance and mixing properties of the atmosphere in several urban regions but they are underestimated or completely neglected in mesoscale weather prediction models.
The motivation of the present study is to understand the phenomena accompanying slope flow during the so called *evening transition*. During the day the flow is directed up-slope (known as the anabatic flow) and at night the reverse flow occurs down the slope (known as the katabatic flow). The transition from up-slope flow to down-slope flow occurs shortly after the sunset, when the ground cooling begins. Recently, Hunt et al. [2] developed an analytical model of the evening transition. It assumes that fluid parcels starting at the bottom break of a slope, which is initially heated and supporting an up-slope flow, are subjected to a gradual cooling of the bottom in linear fashion. As the fluid parcels travel up-slope they become naturally buoyant and finally stop. The stagnation surface of the fluid parcels take the form of a front which subsequently breaks down by heavy fluid parcels which lay above lighter particles behind the front. This new phenomenon has amplifications in air pollution dispersion as the fronts can rapidly mix pollutants vertically and dilute them. Further, on bare lands, such fronts can enliven the dust, thus increasing particulate matter concentrations to unhealthy levels. The possibility of such front formation was demonstrated in the laboratory by Hunt et al. [2], but they did not present information how the temperature of fluid parcels vary along the slope and in the direction normal to the slope.

Therefore, two main objectives of the present work were defined. Firstly, it was to build a small scale laboratory model, permitting detailed measurements of temporary velocity and temperature fields, and to create an experimental database useful for explanation of the flow behaviour typical for the evening transition. Secondly, it was to work out a numerical modelling methodology necessary to predict the temperature and velocity fields obtained from the laboratory model. Simultaneous measurements of both fields by means of the thermochromic liquid crystals tracers [4] facilitated validation of the numerical models.

2. Experimental method

We considered natural convection in a rectangular inclined enclosure filled with water (Fig. 1a). The cavity was of H=38 mm height, D=38 mm depth and L=114 mm length. The four adiabatic side-walls were made from 7.5 mm thick Plexiglas. The other two isothermal side-walls were made of copper. The temperature difference between the isothermal walls were kept at constant value ΔT=6K. The temperatures of the hot wall T_h and cold wall T_c, were 305K and 299K, respectively.
The cavity inclination angle φ varied from 0^o - 90^o. The acquisition system (Fig. 1b) consisted of the 3CCD colour camera (Sony XC003P) and the 32-bit frame grabber (IC-PCI ITI). The flow field was illuminated with a 2 mm thin sheet of white light from a specially constructed 1000 W halogen lamp, and observed in the perpendicular direction. The thermochromic liquid crystal (TLC) tracers, changing colour of refracted light with temperature were employed to measure both temperature and velocity flow fields. The temperature measurements were based on a digital colour analysis of the flow images.

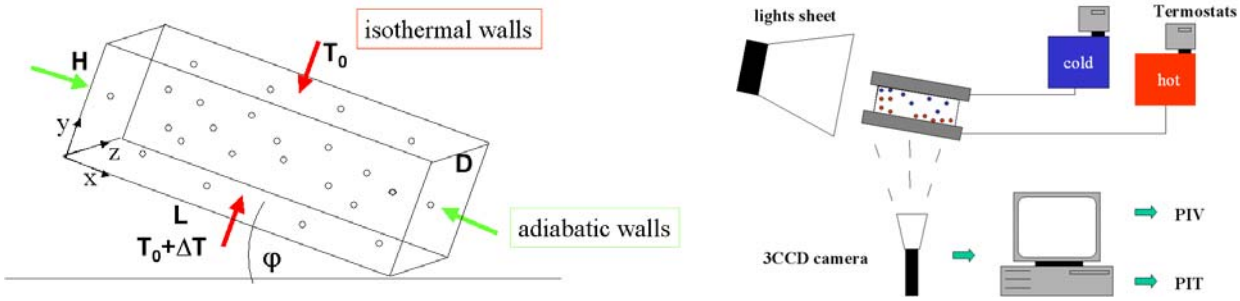

Figure 1: Schematic of the experimental apparatus: (a) – geometry of the cavity with cold and hot isothermal walls indicated, (b) – basic elements of the experimental rig.

The 2D velocity vector field was measured by digital particle image velocimetry (DPIV). By this method, the motion of the scattering particles, observed in the plane of the illuminating light sheet, was analysed by cross-correlating pairs of subsequent images. To get a general view of the flow pattern, several images recorded periodically within a given time interval have been added in the computer memory. Displayed images were similar to the multi-exposed photographs, showing the flow direction and its structure.
The nine thermocouples, T_i (i=1…9) (Fig.2), were used for measurements of the cavity temperature. The thermocouples T1, T2, T3 were placed inside an enclosure and the temperature of water was measured. The temperature of the isothermal walls was measured by remaining six thermocouples. The temperatures were recorded through the Multi Channel Precision Thermometer PTM 3040 (Prema Semiconductor GmbH).

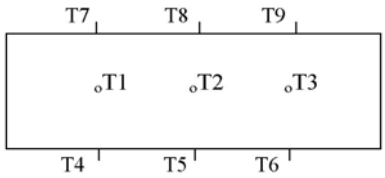

Figure 2: Schematic shows location of the thermocouples monitoring temperature in the cavity.

3. Numerical method

Numerical simulations of the investigated experimental configurations were performed using finite-volume commercial code Fluent 6.1.18 (Fluent Inc., USA). Spatial derivatives were approximated using QUICK scheme, which is based on a weighted average of second-order-upwind and central interpolation of the variable. Pressure-velocity coupling was done using SIMPLE algorithm. Solutions were obtained by direct simulations of the flow for two-dimensional and three-dimensional uniform structural mesh using double precision solver. The solutions were considered to be fully converged when the maximum absolute value of the mass source and the percent changes of the dependent variables at any grid node from iteration to iteration were smaller than a prescribed value, i.e., 10^{-5} and 10^{-6}, respectively.

3.1. Basic equations

The basic equations describing the flow driven by natural convection consist of mass, momentum and energy conservation equations are given by:

$$\frac{\partial u}{\partial x}+\frac{\partial w}{\partial y}=0\,, \tag{3.1.1}$$

$$\rho_0\frac{\partial u}{\partial t}+\rho_0 u\frac{\partial u}{\partial x}+\rho_0 w\frac{\partial u}{\partial y}=-\frac{\partial p}{\partial x}+\mu\Delta u\,, \tag{3.1.2}$$

$$\rho_0\frac{\partial w}{\partial t}+\rho_0 u\frac{\partial w}{\partial x}+\rho_0 w\frac{\partial u}{\partial y}=-\frac{\partial p}{\partial y}+\mu\Delta w\,, \tag{3.1.3}$$

$$\frac{\partial T}{\partial t}+u\frac{\partial T}{\partial x}+w\frac{\partial T}{\partial y}=\alpha\Delta T\,, \tag{3.1.4}$$

The equations presented above describe the two-dimensional incompressible flow, where u, w, ρ_0, p, μ, g, α denote, respectively, the horizontal and vertical velocity, the reference density of fluid, the pressure, the dynamic viscosity, the gravitational acceleration, the temperature and thermal diffusivity, respectively.

3.2. Fluid properties and boundary conditions

Physical properties of water, like density, kinematical viscosity, thermal conductivity, specific heat, thermal expansion coefficient and Prandtl number were assumed constant and their values at the reference temperature T_{ref} = 300 K were used (Table 1).

Table 1: Properties of water used in simulations [5].

	Properties of water at 300 K	Value	Unit
ρ	density of water	1.00 E+03	kg/m^3
ν	kinematical viscosity	8.05 E-07	m^2/s
κ	thermal conductivity	0.6 E+01	W/m·K
Cp	specific heat	4.183E+04	J/kg·K
g	gravitational acceleration	9.81 E+01	m/s^2
β	thermal expansion coefficient	2.77E-04	1/K
Pr	Prandtl number	5.42 E+01	-

Thermal boundary conditions for isothermal walls were T_h=305 K and T_c=299 K for the hot and cold walls, respectively. The Plexiglas walls were assumed adiabatic and the zero heat flux thermal boundary condition was set. The standard no-slip boundary conditions at all walls were adopted for the velocity components. Steady-state and unsteady state solutions were investigated. A uniform fluid temperature of 299K and zero velocity were assumed as the initial conditions.
The Rayleigh (Ra) and Prandtl (Pr) numbers describing investigated configuration were based on the fluid properties taken at the reference temperature, temperature difference ΔT and the cavity height H. For inclined cavity we use the modified Rayleigh number Ra_y , which additionally depends on cosine of the enclosure inclination angle φ.

$$Ra = \Delta T \frac{g \cdot \beta \cdot H^3}{\upsilon^2} \cdot \mathrm{Pr} \tag{3.2.1}$$

$$Ra_y = Ra \cdot \cos\varphi \tag{3.2.2}$$

3.3. Mesh density

Investigated flow configuration covers verity of flow regimes, strongly depending on the selected inclination angle. Due to the flow instabilities, numerical simulation of these regimes is not a trivial task and needs careful verification of results. Hence, the profound tests of mesh dependence were performed to select reliable solutions, to decide if the steady state flow configuration exists, and to find out if two-dimensional simulation is sufficient to reproduce main features of the flow. Table 2 displays optimal mesh sizes found after performing several computational tests, searching for the asymptotic solutions. For 2D unsteady flow model and inclination angles from 70 to 90 deg., the optimal numerical grid consisted of 400*120 cells, but it had to be increased several times as the inclination angle decreased. For the 2D steady-state model the grid density was increased to the value of 800*240 and 1600*480 cells in order to reach the asymptotic behaviour. Investigations of the mesh dependence for 3D simulations were limited by the computational time and computer resources. The maximum acceptable mesh density, three millions elements (100*100*300), appeared to be not adequate to obtain asymptotic 3D solution for all configurations. These not completely verified solutions are hashed in Table 2.

Table 2: Density of numerical meshes selected for the simulations and corresponding modified Rayleigh number Ra_y; # - solutions not fully verified

inclination φ	Ra_y	2D unsteady	2D steady	3D unsteady	3D steady
90	$1.00\ 10^6$	400*120	800*240	50*50*150	50*50*150
80	$1.30\ 10^6$	400*120	800*240	50*50*150	100*100*300
70	$2.56\ 10^6$	400*120	800*240	50*50*150	100*100*300
60	$3.74\ 10^6$	800*120	1600*480	50*50*150	100*100*300
50	$4.81\ 10^6$	800*120	1600*480	100*100*300	100*100*300
40	$5.73\ 10^6$	800*120	1600*480	100*100*300	100*100*300
30	$6.48\ 10^6$	1600*480	#1600*480	#100*100*300	#100*100*300
20	$7.03\ 10^6$	#1600*480	#1600*480	#100*100*300	#100*100*300
10	$7.37\ 10^6$	#1600*480	#1600*480	#100*100*300	#100*100*300
0	$7.48\ 10^6$	#1600*480	#1600*480	#100*100*300	#100*100*300

4. Results and discussion

As a result of experimental and numerical work the temperature and velocity fields for the box with inclination angle φ changed from 0 ° to 90 ° (in 10° steps) were obtained. The experiments were carried out to create the database useful for verification of the numerical results.

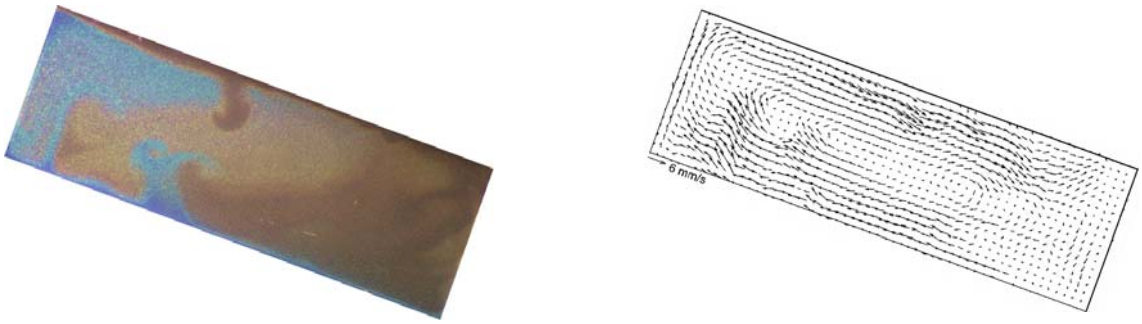

Figure 3: Snap-shots of the temperature and velocity fields observed for the up-slope convection in the cavity at inclination angle $\varphi = 20^{o}$, ΔT=6K (a) - temperature field visualized by TLC tracers (red colour indicates lower temperature), (b) velocity field obtained by cross-correlating pair of tracers images (PIV).

An example of experimental data is presented for the cavity inclination φ = 20° in the Fig.3. It shows visualisation of the instantaneous temperature and the velocity field during generation of the hot and cold plum ejections, forming at the lower and upper wall, respectively. In general, it was observed that these type of instability strongly depends on the cavity inclination and can be only quantitatively reproduced in the numerical model. To obtain general comparison with the numerical simulations, the point measurements of the fluid temperature were used. Figure 4 shows temperature differences $\Delta T_{1\text{-}2}$ and $\Delta T_{2\text{-}3}$, obtained from thermocouples T1, T2 and T3 (comp. Fig. 2) and compared with their numerical counterparts.

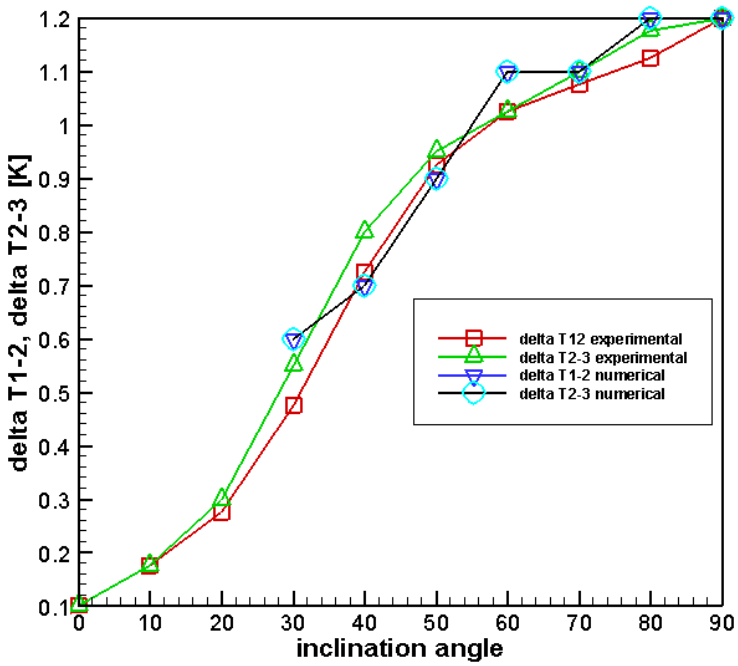

Figure 4 : The influence of inclination angle on difference temperature $\Delta T_{1\text{-}2}$ $\Delta T_{2\text{-}3}$, experimental data compared with the 2D steady state numerical model.

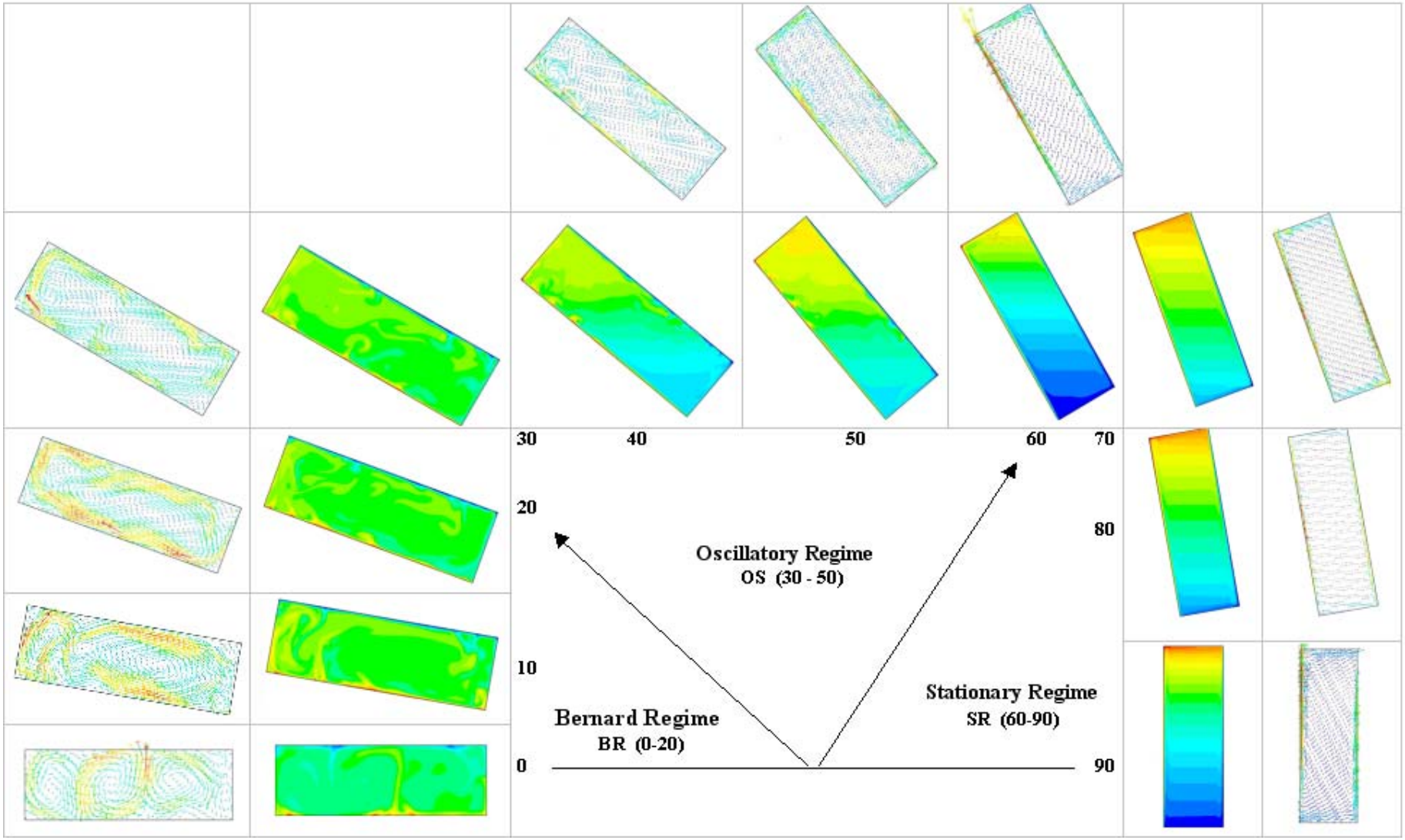

Figure 5: Snap shots from the numerical simulations. Temperature and velocity fields obtained for different inclination angle of the cavity. Three flow regimes: BR – Rayleigh-Benard Regime, OR - Oscillatory Regime, ST-Stationary Regime.

Results displayed in Figure 4 show that numerical simulations correctly reproduced averaged local temperature gradients measured in the cavity, and indicate semi-linear increase of the horizontal temperature stratification for higher inclination angles. Details of the temperature and velocity fields obtained for all investigated configurations are schematically collected in Figure 5. Our parametric study allows us to discriminate three characteristic flow regimes:

1. ST - Stationary Regime, observed for inclination angle form 60 to 90 deg
2. OR - Oscillatory Regime, observed for inclination angle form 30 to 50 deg
3. BR – Rayleigh-Benard Regime, observed for inclination angle from 0 to 20 deg

This classification is obtained from a summary of the numerical results obtained for steady/unsteady, 2D and 3D models. The first, *stationary flow regime* (ST), is compared with the experimental data in Table 3. This regime was defined by comparing results from the steady and unsteady – state solutions. The steady - state solutions were considered to be fully converged when the convergence level of the resolving equations was about 10^{-5} and 10^{-6}. For the unsteady solver the convergence criteria were based on the asymptotic constancy of the averaged temperature and velocity fields. A flow relaxation parameter ($t_{relaxation}$), indicating time necessary to obtain a steady state is given in the Table 3. It is obtained for unsteady solvers with initial conditions set as zero velocity field and uniform fluid temperature. Three velocity maxima obtained from the PIV measurements and two temperatures gradients measured by thermocouples are compared in Table 3 with their numerical counterparts. Beside the global velocity maximum V_{max}, the maximum and minimum values of the y velocity component, $V_{y\ max}$, $V_{y\ min}$, are extracted from the velocity profiles taken along the cavity, in middle of its height (y=H/2). The values of temperature differences ΔT_{1-2}, ΔT_{2-3} are measured with thermocouples as described above.

Table 3: Comparison between numerical and experimental results obtained for inclination angles in the range of 60 – 90 deg (Stationary Regime, ST).

angle 90°	**2D unsteady**	**2D steady**	**3D unsteady**	**3D steady**	**Experiment**
V_{max} m/s	$1.28\ 10^{-2}$	$1.27\ 10^{-2}$	4.610^{-3}	$4.3\ 10^{-3}$	$3\ 10^{-3}$
$V_{y\ max}$ m/s	$1.53\ 10^{-3}$	$1.53\ 10^{-3}$	$7.8\ 10^{-4}$	$7.9\ 10^{-4}$	-
$V_{y\ min}$ m/s	$-1.53\ 10^{-3}$	$-1.53\ 10^{-3}$	$-7.8\ 10^{-4}$	$-7.9\ 10^{-4}$	-
ΔT_{1-2} K	1.2	1.2	1.4	1.2	1.2
ΔT_{2-3} K	1.2	1.2	1.2	1.3	1.2
$t_{relaxation}$ s	570	-	600	-	-
angle 80°					
V_{max} m/s	$1.31\ 10^{-2}$	$1.31\ 10^{-2}$	$4.5\ 10^{-3}$	$4.4\ 10^{-3}$	$3.5\ 10^{-3}$
$V_{y\ max}$ m/s	$2.8\ 10^{-3}$	2.710^{-3}	$1\ 10^{-3}$	$1.1\ 10^{-3}$	-
$V_{y\ min}$ m/s	$-2.8\ 10^{-3}$	$-2.7\ 10^{-3}$	$-1\ 10^{-3}$	$-1.1\ 10^{-3}$	-
ΔT_{1-2} K	1.1	1.1	1.2	1.1	1.1
ΔT_{2-3} K	1.1	1.1	1.2	1.2	1.2
$t_{relaxation}$ s	580	-	700	-	-
angle 70°					
V_{max} m/s	$1.3\ 10^{-2}$	$1.3\ 10^{-2}$	$4.6\ 10^{-3}$	$4.4\ 10^{-3}$	$4\ 10^{-3}$
$V_{y\ max}$ m/s	$4.6\ 10^{-3}$	$4.6\ 10^{-3}$	$1.3\ 10^{-3}$	$1.5\ 10^{-3}$	-
$V_{y\ min}$ m/s	$-4.6\ 10^{-3}$	$-4.6\ 10^{-3}$	$-1.3\ 10^{-3}$	$-1.5\ 10^{-3}$	-
ΔT_{1-2} K	1.1	1.1	1.1	1.1	1.1
ΔT_{2-3} K	1.1	1.1	1.1	1.1	1.1
$t_{relaxation}$ s	590		800		-
angle 60°					
V_{max} m/s	$1.5\ 10^{-2}$	$1.4\ 10^{-2}$	$4\ 10^{-3}$	$4\ 10^{-3}$	$4.5\ 10^{-3}$
$V_{y\ max}$ m/s	$7.7\ 10^{-3}$	$7\ 10^{-3}$	$1.6\ 10^{-3}$	$1.9\ 10^{-3}$	-
$V_{y\ min}$ m/s	$-7.5\ 10^{-3}$	$-7\ 10^{-3}$	$-1.6\ 10^{-3}$	$1.9\ 10^{-3}$	-
ΔT_{1-2} K	1.1	1	1	1	1
ΔT_{2-3} K	1.2	1	1	1	1
$t_{relaxation}$ s	620	-	900	-	-

The table shows increase of the flow relaxation time for 3D simulations in comparison with 2D solutions. These differences became even larger for higher values of the inclination angle. It indicates that three-dimensionality of the flow structures has to be taken into account in the numerical simulations. Similar conclusion can be drawn by comparing velocity maxima of measured and simulated fields. The three-dimensional simulation overestimates measured values by about 20%, whereas values obtained from the two-dimensional simulations are almost one order of magnitude higher than experimental. It appears that despite simple geometry, the analysed flow is strongly three-dimensional. The flow structure depends on the flow interaction with the side walls, evidently decreasing velocity components in the (x, y) symmetry plane.

Figure 6 displays comparison of several numerical simulations performed with two- and three-dimensional models. The velocity profiles were extracted along the cavity in the middle of the centre cross-section (y=0.5). They illustrate up flow along the top wall, with a distinct velocity maximum, and similar reverse flow along the bottom wall. By varying inclination of the cavity the maximum velocity decreases. Similar behaviour can be found in the both two- and three-dimensional models. But in all investigated inclinations the velocity maximum close to the side walls is almost three times lower for three-dimensional model (Fig. 6b) than for two-dimensional one (Fig. 6a).

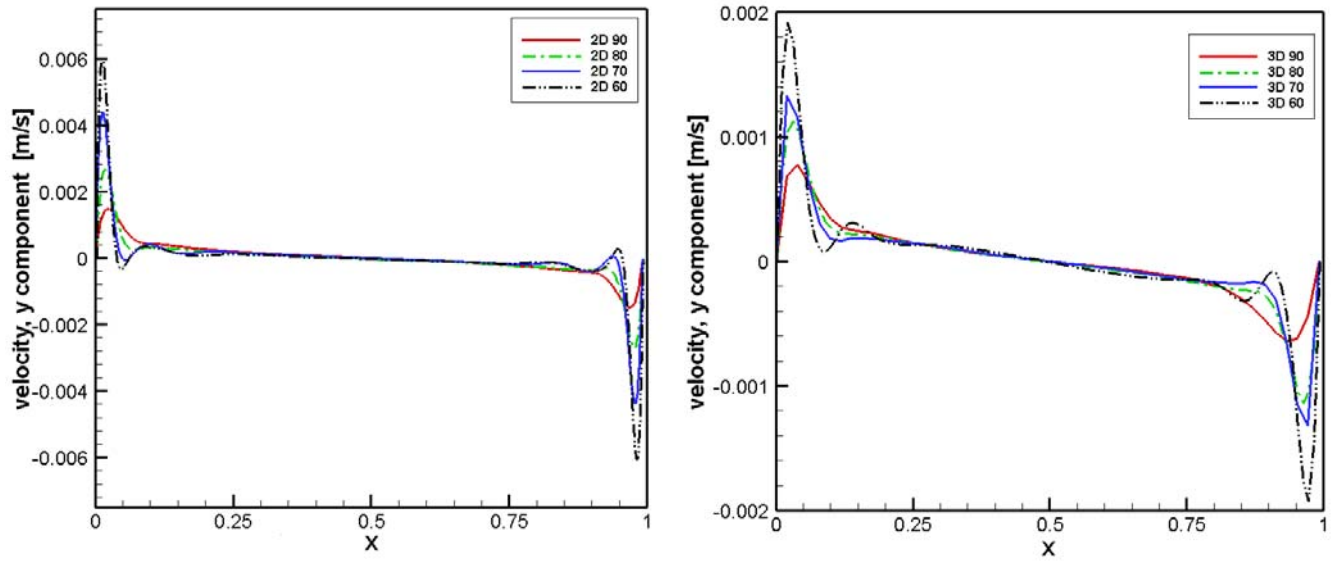

(a) (b)

Figure 6: Profiles of the y velocity component extracted along cavity for the centre-line y=0.5; x - non-dimensional distance from the top wall. (a) – solution for 2D steady-state model, (b) – solution for 3D steady-state model.

For smaller inclination angles, from 30 to 50 deg, the oscillatory flow regime starts. It was clearly visible in the experiments, where periodic bursts of hot and cold plums separated from the both isothermal walls. Such bursts are well visible in the snap shots from numerical simulations collected in Fig. 5. The observed flow unsteadiness enforces application of unsteady numerical solvers and statistical analysis of the flow characteristics. Further decrease of the inclination angle gradually transforms flow into the third, Rayleigh-Bendard type regime. It is characterized by development of more or less regular recirculation rolls, with two or three cross-flow rolls and possible longitudinal rolls in the both cavity extremes. The flow structure remains time-dependent; location of the convection rolls varies in time. This flow regime is the most typical for the atmospheric flow over natural elevations. The numerical simulations confirm qualitatively presence of the flow structures observed in the experiments made for small inclinations (comp. Fig. 3 and 5). However, fluctuating nature of observed and simulated velocity fields did not allow us to perform any quantitative comparisons. More detailed investigations of both unsteady flow regimes are aimed in the further work.

Conclusions

The effect of inclination on natural convection of water in a rectangular enclosure with aspect ratio A_x=3 was investigated numerically and experimentally for angles from 0 to 90 deg relative to the vertical. For each inclination the temperature difference between two opposite, isothermal walls (bottom-hot, upper-cold) was kept constant and equal 6^{o}C. The PIV and PIT techniques were used to collect full field data on temperature and velocity in the centre cross-section of the cavity. The several steady, unsteady, 2D and 3D numerical models were applied to simulate investigated configurations. The parametric numerical study designates three distinct flow regimes, the steady state flow regime for high cavity inclinations (90-60 deg), the oscillatory flow regime for intermediate inclinations (50-30 deg) and the transition to Rayleigh-Bénard flow regime for small inclinations (20-0 deg). Experimental results and numerical simulations performed for the first flow regime indicate strong three-dimensionality of the flow structure, excluding possibility for simplified, two-dimensional numerical modelling. The two remaining flow regimes appeared to be strongly time-dependent and only qualitative comparison with the experiments was presently available.

References

[1] S. Ostrach, Natural convection in enclosures, J. Heat Transfer 110 (4-B) 1988 1175-1190
[2] J.C.R. Hunt, H.J.S. Fernando, M. Princevac, Unsteady Thermally Driven Flows on Gentle Slopes, *J. Atmospheric Sci.* 60, 2169-2182, 2003
[3] P. Monti, H.J. Fernando, M. Princevac, T.A. Kowalewski, W.C. Chan, E.R. Padyjak, Observations of flow and turbulence in the nocturnal boundary layer, *J. Atmospheric Sci.* 59, 2513-2534, 2002
[4] T.A. Kowalewski, Application of liquid crystals for full field temperature and velocity measurements, *Proc. of the Inter. Symp. on Environ. Hydr.*, ASU Tempe 2001, CD-ROM, p.154.1-6, 2001
[5] K. Dekajlo, T. A. Kowalewski, Experiment on up-slope to down-slope transition in an inclined box filled with water, CD-ROM Proceedings of 21st ICTAM in Warsaw, FM9S_10576, p.102, 2004
[6] F.P. Incopera, D.P. de Witt, Fundamentals of Heat and Mass Transfer, 1990, appendix A